REPOSITORIO UNIVERSIDADE CORUÑA

UNIVERSIDADE DA CORUÑA

This is the ACCEPTED VERSION of the following published document:

Estefanía Rivas Vázquez, María Noelia Barreira Rodríguez, Emilio López-Varela, Manuel G. Penedo, "Deep learning for segmentation of optic disc and retinal layers in peripapillary optical coherence tomography images," Proc. SPIE 12701, Fifteenth International Conference on Machine Vision (ICMV 2022), 127011A (7 June 2023); https://doi.org/10.1117/12.2680545

Link to published version: https://doi.org/10.1117/12.2680545

General rights:

This version of the conference paper has been accepted for publication, after peer review in Proceedings SPIE 12701, Fifteenth International Conference on Machine Vision (ICMV 2022), 127011A, but is not the Version of Record and does not reflect post-acceptance improvements, or any corrections. The Version of Record is available online at: https://doi.org/10.1117/12.2680545.

Deep Learning for Segmentation of Optic Disc and Retinal Layers in Peripapillary Optical Coherence Tomography Images

Estefanía Rivas Vázquez[a], María Noelia Barreira Rodríguez[b,c], Emilio López-Varela[b,c], and Manuel G. Penedo[b,c]

[a]University of A Coruña, A Coruña, Spain
[b]INIBIC, VARPA Group, University of A Coruña, Elviña Campus, 15006, A Coruña, Spain
[c]CITIC, University of A Coruña, Elviña Campus, 15071, A Coruña, Spain

ABSTRACT

Optical coherence tomography (OCT) is a non-invasive technique that allows the retina to be studied with precision, the analysis of the features of its layers and other structures such as the macula or the optic nerve. This is why it is used in the diagnosis and monitoring of eye diseases such as glaucoma and optic neuritis. A crucial step in this process is the segmentation of the different layers, which is a great challenge due to its complexity. In this work, a methodology based on deep learning and transfer learning will be developed to automatically segment nine retinal layers in OCT images centred on the optic disc. In addition, the thickness of each retinal layer will be measured along each B-scan. For this purpose, OCT images from a public dataset and a dataset collected from depth-enhanced images will be used. The proposed method achieves a Dice score of 83.6%, similar to that obtained in the state of the art, segmenting the nine retinal layers and the optic disc in both sets of images. In addition, the different layers are represented in three different graphical formats.

Keywords: peripapillary OCT, layer segmentation, thickness measurement

1. INTRODUCTION

Optical coherence tomography (OCT)[1] is a non-invasive imaging modality that provides high-resolution images of the retina. Using this technique, a sequence of two-dimensional (2D) images with micrometre resolutions is generated based on the optical dispersion properties of near-infrared light in biological tissues.[2] In these, it is possible to directly view the layered structure of the retina and to measure the thickness of each of its layers.

The introduction of domain optical coherence tomography (SD-OCT) makes it possible to obtain high-resolution images of the retina. Thus, SD-OCT can be centred on the optic nerve (ONH) or on the macula, most commonly used option. A fundus image with the different B-scans and a particular section centred on macula (left) or optic disc (right) is shown in Fig. 1. The high resolution of OCT together with other advantages such as its low cost, ease of use and non-invasiveness make it essential in medical specialties such as ophthalmology and neurology. Moreover, numerous studies have confirmed the correlation between abnormalities in the retinal layers with the presence of diseases such as multiple sclerosis, type 1 diabetes, Alzheimer's disease, Parkinson's disease and glaucoma, among others. Therefore, accurate tissue segmentation of OCT images of the retina becomes a fundamental step in the early diagnosis of these diseases.

Histologically, the retina consists of thirteen layers from inner to outer (Fig. 2): inner limiting membrane (ILM), retinal nerve fibre layer (RNFL), ganglion cell layer (GCL), inner plexiform layer (IPL), inner nuclear layer (INL), outer plexiform layer (OPL), outer nuclear layer (ONL), outer limiting membrane (ELM), photoreceptor

Further author information: (Send correspondence to E.R.V.)
E.R.V.: E-mail: estefania.rv.24@gmail.com
M.N.B.R.: E-mail: noelia.barreira@udc.es
E.L.V.: E-mail: e.lopezv@udc.es
M.G.P.: E-mail: mgpenedo@udc.es

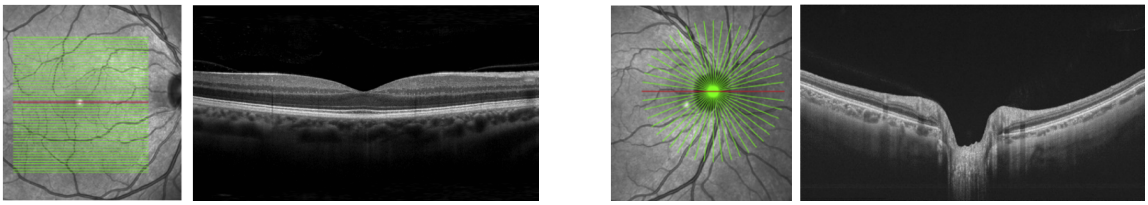

Figure 1. A fundus image with multiple horizontal lines, representing the locations of each B-scan, and the second a two-dimensional image centred on the macula (red line). The next two images represent a fundus image with multiple radial lines through the optic nerve and a two-dimensional image centred on the optic disc (red line).

layers (PR), retinal pigment epithelium (RPE), Bruch's membrane (BM), choroidal capillaries (CC) and choroidal stroma (CS). As can be seen in the image, manual segmentation of these layers is a laborious task, so in recent years, accurate automated segmentation has been sought using algorithms based on changes in reflectivity between adjacent structures.

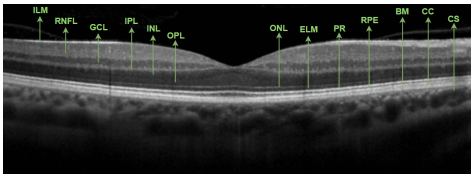

Figure 2. Macular centred OCT showing the thirteen layers of the retina

The main objective of this work is to develop and validate a methodology to automatically segment retinal layers in OCT images centred on the optic disc. Subsequently, the thickness of each retinal layer will be measured along the B-scan. To test the robustness and efficiency of the method, experiments are performed with two different data sets. Thus, a public dataset will be used to compare the approach with the state of the art and a dataset collected from enhanced depth imaging (EDI) will be used for the visualisation part of the results.

2. STATE OF THE ART

Over the years, different techniques of variable complexity have been proposed for the segmentation of retinal layers. Ref. 3, 4 present methods for segmenting spectral OCT images based on graph theory, where the first one incorporates texture features. Later, in 2013, a classifier was proposed that segmented eight retinal layers in macula-centred OCT images. This work was followed by other models using active contour segmentation methods.[5] In recent years, the power of deep learning-based convolutional neural networks (CNNs) for image segmentation of various modalities has been demonstrated. Two of the most widely used networks for this purpose are Fully Convolutional Networks (FCN) and the UNet. One of the first published papers proposing a deep learning-based method for automated segmentation of retinal OCT images was by 6 in 2017. Subsequently, 7 developed a model combining CNN and graph search methods for the segmentation of nine retinal layers in OCT images.

All the methods discussed so far perform segmentation on macula-centred OCT images. Research for the segmentation and analysis of optic nerve-centred OCT image layers has not reached the same level of development. In 8 an combination of a convolutional neural network with a graph search algorithm was used to detect the retinal layer boundaries. Following this work, several models based on it are proposed. In this way, 9 proposed a model that used graph theory for the segmentation of the optic disc boundary in an image previously generated from the Bruch's membrane. 10 combined graph search methods with the active appearance model (AAM). 11 applied a UNet-type network that succeeds in segmenting five retinal layers, but falls short of completely delimiting the optic disc.

A major factor is that all of the above methods for analysing optic disc-centred OCT images do not clearly consider the existence of the optic disc, making layer segmentation more error-prone near this central region. Specifically, the region deep within the optic disc is different from the other regions, causing the segmented

surfaces to deviate from their actual locations near the edge of the hole. In addition, the retinal layers are arranged vertically with different thicknesses between them, creating a discontinuity that makes segmentation of the layers difficult. This is why the presence of the optic disc in the images represents a great increase in the complexity of the problem as it is an area with very different characteristics to the rest of the retina. Therefore, it is important to design a model that is able to detect both parts (disc and non-disc) efficiently. Therefore, a two-stage assisted convolutional graph network (CNG) was proposed for joint segmentation of the retinal and optic disc layers in peripapillary OCT images. In this last work, they were able to significantly improve the segmentation of the optic disc and layers compared to previous published work.

3. MATERIALS AND METHODS

3.1 Datasets and Software resources

Two different datasets are used to perform the experiments, where all images share a similar anatomical layout, where the optic disc is located in the central region of the image and the different stratified layers are on either side of it.

To prove the efficacy of the model, experiments are performed on the public dataset collected by 12 optic disc-centred OCT from 61 subjects using the DRI OCT-1 Atlantis (Topcon Corporation, Tokyo, Japan). This dataset consists of 244 images with 992×1024 resolution. Each image has its corresponding mask, where an expert manually labelled the optic disc region and the boundaries of the different retinal layers. Fig. 3 shows the labels of the optic disc and the nine retinal layers selected for segmentation in this work, where IS/OS refers to the inner/outer photoreceptor segment. In addition, another optic disc-centred OCT dataset obtained from 40 individuals at the Ophthalmology Service of the Ferrol University Hospital Complex (Spain) will be used. For each subject there are two OCT cubes, created using two equivalent Spectralis R OCT capture devices from Heidelberg Engineering, where one belongs to the right eye and the other to the left eye. Each radial OCT cube consists of 27 slices centred on the peripapillary region with an image resolution of 768×496. In addition, each includes two or three images of circular slices centred on the optic disc. It is in these last images that the capture device performs the segmentation of retinal layers, but it only manages to delimit three of them: RNFL, GCL and ganglion cell complex (GCC; GCL + IPL).[13] Fig. 3 also shows the two types of images extracted from each of the two datasets. Note how in the second case the slices cover a smaller area on both sides of the optic disc. Besides, the different arrangement of the optic disc in the images can be observed.

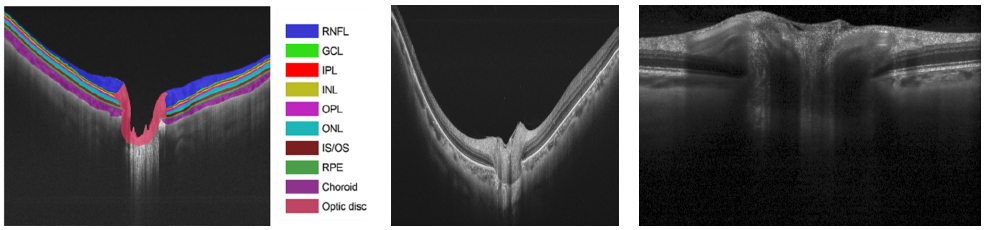

Figure 3. Manual labelling of a peripapillary OCT image of the set in 12. The optic disc region and the nine retinal layers are displayed on the original image in different colours. The last two images show an example of OCT image of the first dataset and an OCT image of the second dataset.

This work has been developed in Python 3.8.12 with the framework of TensorFlow 2.8.0 and Keras 2.8.0 as well as the segmentation-models library.[14] Image processing libraries such as OpenCV (4.5.5.64), Numpy (1.22.2) and Scikit-Image (0.19.2) are also used.

3.2 Network architecture

The aim of this work is to develop a methodology based on convolutional neural networks to segment the optic disc and nine layers of the retina. The UNet,[15] widely used in computer vision segmentation, is used as the base architecture. This type of FCN is characterised by a symmetrical architecture consisting of an encoder and a decoder connected by concatenations and transposed convolutions to combine channels. Feature maps

are progressively extracted at different scales, which are jointly used to perform the final model prediction. By following this scheme, a more accurate segmentation of the different objects and their boundaries is achieved.

To address the goal of segmenting the different layers of the retina and the optic disc, transfer learning is applied by using a pre-trained network as a basis. This option is useful to avoid overfitting in cases where the size of the data set is small. An important step in designing the convolutional network is to select a good encoder to find the best segmentation. Therefore, two different encoder configurations with different characteristics and number of parameters are tested. These encoders are part of neural architectures commonly used in similar application domains. The first one is the densely-connected convolutional network (DenseNet)[16] which is based on the progressive concatenation of features from previous layers to enforce feature propagation. Specifically, in this work, DenseNet169 was used as the encoder. On the other hand, we tested the EfficientNet[17] network, which corresponds to a family of models created by balancing the depth, width and resolution of the network efficiently and effectively. In this work, EfficientNetb0 was used as the encoder.

3.3 Training details

The public dataset with the parameters and splitting specified in the original work is used.[12] Specifically, this dataset is divided into training set (148 images), test (48 images) and validation (48 images), where all images have a resolution of 992×1024. The images for the network input were resized to 512×512 and the number of channels was modified from 1 to 3. The data from the training, validation and test set was normalised and standardised so that all images have the same dimensions. The learning rate was set to 0.001 and the Adam optimiser was used. Each of the models was trained on the dataset with a batch size of 1 (due to the available memory) and for a maximum number of 3000 epochs, using the early stopping parameter with a patience of 30. This parameter stops the training process when no improvement in the evaluation metric is observed in the validation set. Thus, overfitting of the network is avoided.

As a loss function, the combination of two functions was used: the Dice loss and the categorical focal loss (CFL) (Equation 1), where g_i and p_i indicate the *ground truth* and the probability in the prediction that the pixel x belongs to the class i respectively, and M is the number of classes in the segmentation network. Regarding model evaluation, all models were evaluated in two ways. Specifically, for the set of test images, the Dice score (DSC) and the Jaccard score (J) were obtained (Equation 2), where X represents the prediction region and Y is the *ground truth* region.

$$Dice = 1 - \frac{1}{M}\sum_{i=1}^{M}\left(\frac{2\sum_{x\in\Omega} p_i(x)\cdot g_i(x)}{\sum_{x\in\Omega} p_i(x) + \sum_{x\in\Omega} g_i(x)}\right) \qquad CFL(p_t) = -g_i\alpha(1-p_t)^{\gamma}log(p_t) \tag{1}$$

$$DSC = \frac{2\cdot|X\cap Y|}{|X|+|Y|} \qquad J = \frac{|X\cap Y|}{|X\cup Y|} \tag{2}$$

3.4 Calculation of retinal layer thicknesses

Prior to the calculation of the thickness of the individual retinal layers, the OCT images of both data sets were post-processed. Due to the non-horizontal arrangement of the different retinal layers with respect to the abscissa axis and in order to simplify the calculation of the thickness of each one of them, the image was flattened. After the layer segmentation and the removal of the optic disc region, the retinal layer to be used as the baseline for the calculation of the displacement vectors is selected. For this purpose, the layer with the best segmentation in all the images is sought, being the ONL in the case of the public dataset, and the OPL in the second dataset. Then, the bottom line of the mask of the selected layer is selected and the displacement of each pixel is calculated, corresponding to the distance from the centre of the image to the line. Finally, the flattening algorithm is applied using the nearest neighbour interpolation method. Thus, the different retinal layers in the resulting image are arranged parallel to the abscissa axis. Finally, the thickness of the individual retinal layers is calculated. To do this, the upper and lower line is calculated for each layer and then the thickness in pixels is calculated as the difference between the two lines. In the case of the B-scans of the second dataset, the information needed to obtain the ratio of pixels to micrometres is available so the thickness in μm can be calculated.

3.5 Visualisation

After literature review, the thickness of each retinal layer in the different B-scans was represented by using three types of graphs. In the first one, the thickness in pixels or μm of each layer is represented linearly. The second one represents the same as the previous one, but using a stacked area plot. This last form of representation allows us to study the relationship between each of the retinal layers in a simpler way. Finally, a pie chart shows the global and average thickness in each of the retinal layers in each concentric division of the eye. To do this, the line graph previously obtained is divided into four parts of 80 pixels or μm each and the average is calculated in each of them. The second and fourth parts are further divided in half, so that finally there are eight parts of variable size between 80 and 40 pixels or μm.

4. RESULTS AND DISCUSSION

4.1 Segmentation of retinal and optic disc layers

Fig. 4 shows an example of segmentation obtained in each of the two configurations using one of the images from the first dataset as an example.

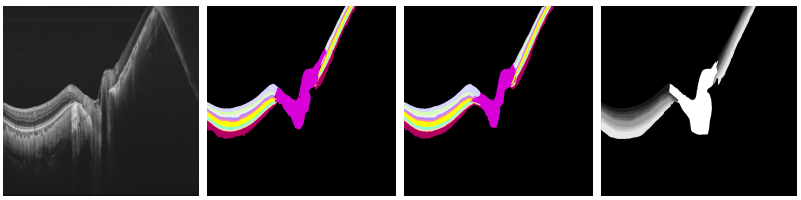

Figure 4. Example of the resulting segmentations in the DenseNet169 and EfficientNetb0 configurations. The last image shows the ground truth.

Table 1 shows the values of the two evaluation metrics for each of the segmented retinal layers using DenseNet169 as the encoder. The last two columns show the values obtained for the segmentation evaluation metrics using the two combinations. It can be seen that the results of the Dice and Jaccard coefficients are similar in both cases, but are slightly higher in the case of using EfficientNetb0 as the encoder. Besides, the global metrics obtained by the model using DenseNet169 are lower than the metrics in some of the layers (ONL, IS/OS and choroid) and the ones in the optic disc.

Table 1. Global values and values obtained in the segmentation evaluation metrics for each retinal layer, optic disc and background. Where BG is background and DN and EN are DenseNet169 and EfficientNetb0 respectively.

Class	RNFL	GCL	IPL	INL	OPL	ONL	IS/OS	RPE	Choroid	Optic disc	BG	DN	EN
DSC	0.832	0.675	0.707	0.757	0.805	0.908	0.864	0.825	0.893	0.846	0.959	0.834	0.836
J	0.716	0.522	0.554	0.615	0.678	0.833	0.769	0.710	0.819	0.743	0.922	0.727	0.733

The trained network has been tested with the second dataset for which ground truth is not available. Specifically, the network with DenseNet169 encoder is used because it shows less possible overfitting in the learning step. In this case, since we are dealing with images with a size of 768×496, different rescaling methods were tested in order to adapt them to the input of the network. Specifically, the best result was obtained after adding a black border around the image, increasing the resolution to 992×1024, and then rescaling to 512×512. In Fig. 5, the lower left image shows the segmentation obtained in one of the images of this dataset. We can see how it is of lower quality than the one obtained with the first dataset. This difference is due to the poorer resolution of the images of the latter dataset, as well as the different arrangement of the slice in the image. In this case, it is not possible to calculate the segmentation evaluation metrics since the masks of the images are not available.

4.2 Calculation of layer thickness and visualisation

Fig. 5 shows a comparison between the output of the network versus the result of applying the flattening algorithm to one of the images in each dataset. It can be seen how the different retinal layers are now arranged parallel to the abscissa axis of the image.

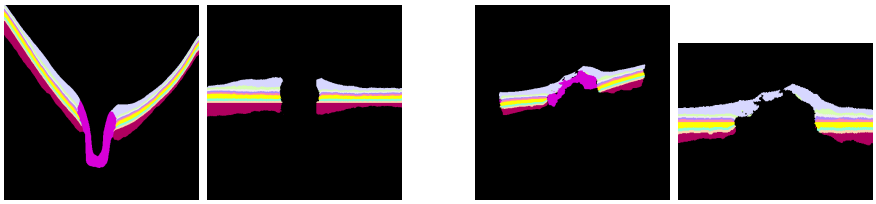

Figure 5. The first two images show an example of segmentation of one of the images from the first dataset and the result of applying the flattening algorithm to it. The last two show the same, but using an image from the second dataset.

Fig. 6 shows a line plot and a stacked area plot representing the thickness in pixels along one of the images of the first dataset. In both graphs it was decided to eliminate the last layer of the retina (choroid) since it has been observed that its presence hinders the visualisation of both graphs. In the central part of the graphs, the thicknesses of the different retinal layers show a value of zero, indicating the presence of the optic disc in this region. The stacked area graph shows how all the layers, except for the RNFL layer, have a constant thickness throughout the B-scan.

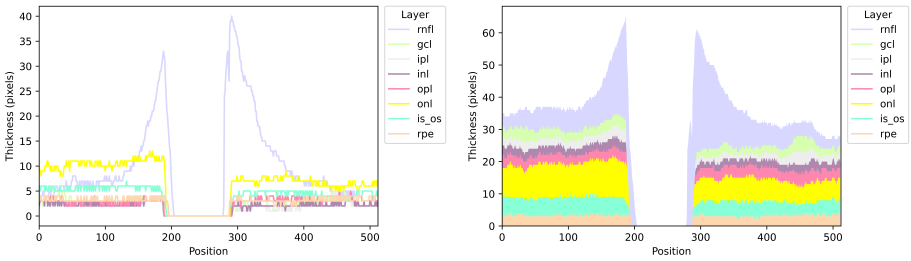

Figure 6. Line plot (left) and stacked area plot (right) for an example image of the first data set.

Fig. 7 shows for an example B-scan, its location, its line graph and the stacked area plot corresponding to each eye of one of the individuals in the second data set. The line plots show the thickness in pixels of each of the layers, but unlike the ones of the first set, in this case there is not such a clear region where the thicknesses have a value of zero. Again, this is due to the poorer resolution of the images in this second dataset. For this reason, it is decided to use the OPL layer as a boundary in order to be able to visualise the location of the optical disc more clearly in the stacked area plot which shows the total thickness of the retina broken down into its layers. In both plots, the thickness decreases as the layers get closer to the optical disc.

Finally, the corresponding pie charts using the fifth retinal layer (OPL) as an example are shown in Fig. 8. They show the overall and average thickness in each of the parts into which each B-scan (Fig. 7) was divided. It can be seen that the overall thickness in both eyes is very similar. Moreover, the results support the observations in the two previous graphs, since where the optic disc is located, the thickness of the layer is lower.

5. CONCLUSIONS

Segmentation of peripapillary OCT images is more challenging due to the variable features of both optic disc and retinal layers. In this paper we propose a methodology to segment nine retinal layers and the optic disc using a pre-trained UNet-type network with an DensenNet169 and EfficientNetb0 encoder. The method is tested on two different datasets. Experimental results on the first dataset show that this simple network developed with robust encoders and transfer learning obtains results comparable to the state of the art. Specifically, the proposed method presents a Dice score of the optic disc segmentation and retinal layers of 83.6%, similar to other state-of-the-art based solely on deep learning techniques ($80\% - 88,1\%$). Although the segmentation is not improved in all the layers, an improvement is observed in the RNFL, IS/OS and choroid layers with respect to the results obtained in the paper with the best Dice rates/values. In addition, the visual quality of the segmented images from both data sets is significantly improved. This, together with the different graphical representations of the thickness of each layer, helps the clinician in the diagnosis and monitoring of diseases such as multiple sclerosis and glaucoma, reducing the subjectivity related to the latter.

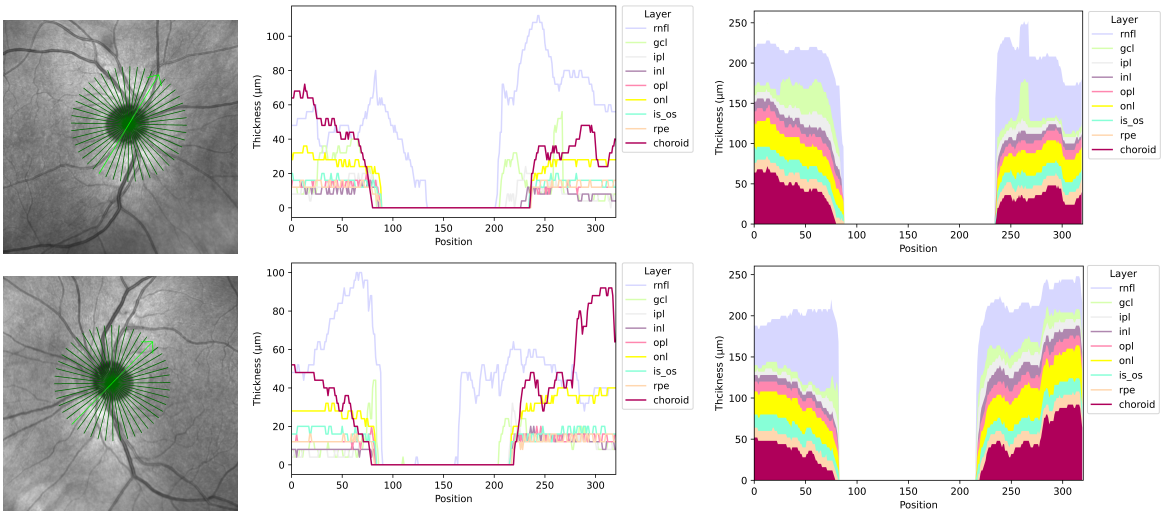

Figure 7. Location of the B-scan (green arrow) and its corresponding line plot and stacked area plot for the right (first row) and left (second row) eye of one of the individuals in the second dataset.

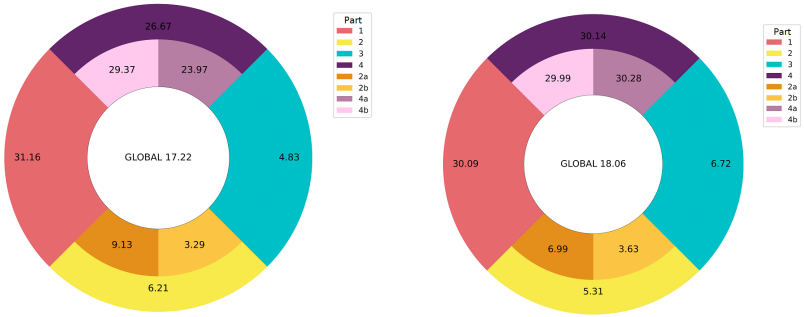

Figure 8. Pie chart showing the mean outer plexiform layer (OPL) thickness in microns for each sector of right and left eye. The overall mean is shown in the centre.

In the future, we will try to analyse the results in images of different resolutions. Also, we will aim to develop a dataset with more segmented layers and test this type of network on these images.

ACKNOWLEDGMENTS

This research was funded by Instituto de Salud Carlos III, Government of Spain, DTS18/00136 research project; Ministerio de Ciencia e Innovación y Universidades, Government of Spain, RTI2018-095894-B-I00 research project; Ministerio de Ciencia e Innovación, Government of Spain through the research project with reference PID2019-108435RB-I00; Consellería de Cultura, Educación e Universidade, Xunta de Galicia, Grupos de Referencia Competitiva, grant ref. ED431C 2020/24; Axencia Galega de Innovación (GAIN), Xunta de Galicia, grant ref. IN845D 2020/38; CITIC, Centro de Investigación de Galicia ref. ED431G 2019/01, receives financial support from Consellería de Educación, Universidade e Formación Profesional, Xunta de Galicia, through the ERDF (80%) and Secretaría Xeral de Universidades (20%).

REFERENCES

[1] D. Huang, E. A. Swanson, C. P. Lin, J. S. Schuman, W. G. Stinson, W. Chang, M. R. Hee, T. Flotte, K. Gregory, C. A. Puliafito, *et al.*, "Optical coherence tomography," *science* **254**(5035), pp. 1178–1181, 1991.

[2] D. L. Budenz, D. R. Anderson, R. Varma, J. Schuman, L. Cantor, J. Savell, D. S. Greenfield, V. M. Patella, H. A. Quigley, and J. Tielsch, "Determinants of normal retinal nerve fiber layer thickness measured by stratus oct," *Ophthalmology* **114**(6), pp. 1046–1052, 2007.

[3] M. K. Garvin, M. D. Abramoff, X. Wu, S. R. Russell, T. L. Burns, and M. Sonka, "Automated 3-d intraretinal layer segmentation of macular spectral-domain optical coherence tomography images," *IEEE transactions on medical imaging* **28**(9), pp. 1436–1447, 2009.

[4] S. J. Chiu, X. T. Li, P. Nicholas, C. A. Toth, J. A. Izatt, and S. Farsiu, "Automatic segmentation of seven retinal layers in sdoct images congruent with expert manual segmentation," *Optics express* **18**(18), pp. 19413–19428, 2010.

[5] I. Ghorbel, F. Rossant, I. Bloch, S. Tick, and M. Paques, "Automated segmentation of macular layers in oct images and quantitative evaluation of performances," *Pattern Recognition* **44**(8), pp. 1590–1603, 2011.

[6] A. G. Roy, S. Conjeti, S. P. K. Karri, D. Sheet, A. Katouzian, C. Wachinger, and N. Navab, "Relaynet: retinal layer and fluid segmentation of macular optical coherence tomography using fully convolutional networks," *Biomedical optics express* **8**(8), pp. 3627–3642, 2017.

[7] L. Fang, D. Cunefare, C. Wang, R. H. Guymer, S. Li, and S. Farsiu, "Automatic segmentation of nine retinal layer boundaries in oct images of non-exudative amd patients using deep learning and graph search," *Biomedical optics express* **8**(5), pp. 2732–2744, 2017.

[8] P. Zang, S. S. Gao, T. S. Hwang, C. J. Flaxel, D. J. Wilson, J. C. Morrison, D. Huang, D. Li, and Y. Jia, "Automated boundary detection of the optic disc and layer segmentation of the peripapillary retina in volumetric structural and angiographic optical coherence tomography," *Biomedical optics express* **8**(3), pp. 1306–1318, 2017.

[9] Z. Hu, M. Niemeijer, K. Lee, M. D. Abramoff, M. Sonka, and M. K. Garvin, "Automated segmentation of the optic disc margin in 3-d optical coherence tomography images using a graph-theoretic approach," in *Medical Imaging 2009: Biomedical Applications in Molecular, Structural, and Functional Imaging*, **7262**, pp. 223–233, SPIE, 2009.

[10] E. Gao, F. Shi, W. Zhu, C. Jin, M. Sun, H. Chen, and X. Chen, "Graph search: active appearance model based automated segmentation of retinal layers for optic nerve head centered oct images," in *Medical Imaging 2017: Image Processing*, **10133**, pp. 495–502, SPIE, 2017.

[11] S. K. Devalla, P. K. Renukanand, B. K. Sreedhar, G. Subramanian, L. Zhang, S. Perera, J.-M. Mari, K. S. Chin, T. A. Tun, N. G. Strouthidis, *et al.*, "Drunet: a dilated-residual u-net deep learning network to segment optic nerve head tissues in optical coherence tomography images," *Biomedical optics express* **9**(7), pp. 3244–3265, 2018.

[12] J. Li, P. Jin, J. Zhu, H. Zou, X. Xu, M. Tang, M. Zhou, Y. Gan, J. He, Y. Ling, *et al.*, "Multi-scale gcn-assisted two-stage network for joint segmentation of retinal layers and discs in peripapillary oct images," *Biomedical Optics Express* **12**(4), pp. 2204–2220, 2021.

[13] J. M. Martinez-de-la Casa, P. Cifuentes-Canorea, C. Berrozpe, M. Sastre, V. Polo, J. Moreno-Montanes, and J. Garcia-Feijoo, "Diagnostic ability of macular nerve fiber layer thickness using new segmentation software in glaucoma suspects," *Investigative ophthalmology & visual science* **55**(12), pp. 8343–8348, 2014.

[14] P. Yakubovskiy, "Segmentation models pytorch." https://github.com/qubvel/segmentation_models.pytorch, 2020.

[15] O. Ronneberger, P. Fischer, and T. Brox, "U-net: Convolutional networks for biomedical image segmentation," in *International Conference on Medical image computing and computer-assisted intervention*, pp. 234–241, Springer, 2015.

[16] G. Huang, Z. Liu, L. van der Maaten, and K. Q. Weinberger, "Densely connected convolutional networks," in *Proceedings of the IEEE Conference on Computer Vision and Pattern Recognition (CVPR)*, July 2017.

[17] M. Tan and Q. Le, "Efficientnet: Rethinking model scaling for convolutional neural networks," in *International conference on machine learning*, pp. 6105–6114, PMLR, 2019.

AUTHORS' BACKGROUND

Your Name	Title	Research Field	Personal website
Estefanía Rivas Vázquez	Master student	Biomedical engineering	estefania.rv.24@gmail.com
María Noelia Barreira Rodríguez	Full professor	Computer Science	noelia.barreira@udc.es
Emilio López-Varela	PhD canditate	Computer Science	e.lopezv@udc.es
Manuel G. Penedo	Full professor	Computer Science	mgpenedo@udc.es